Performance Analysis of a Combined Cycle Power Plant with Simultaneous Cooling of Inlet Air Streams to the Compressor and Condenser

Ifeanyi Henry Njoku*, Chika Oko and Joseph Ofodu

Department of Mechanical Engineering, Faculty of Engineering,
University of Port Harcourt, Choba, Port Harcourt, Nigeria

*Corresponding Author: E-mail: njokuhi@gmail.com
Phone:+234-8033403718

Abstract: This paper presents the thermodynamic performance analysis of an existing combined cycle power plant to be retrofitted with a waste heat driven aqua lithium bromide absorption refrigerator for cooling the inlet air streams to the compressor and air-cooled steam condenser. The power plant is located in the hot and humid tropical region of Nigeria, latitude 4°45′N and longitude 7°00′E. This was achieved by performing energy and exergy analysis of the integrated system. Using the operating data of the existing combined cycle power plant, the results of the analysis showed that by cooling the inlet air streams to 15°C at the compressors, and to 29°C at the air-cooled steam condenser, the net power output, thermal and exergy efficiencies of the combined cycle plant increased by 7.7%, 8.1% and 7.5% respectively while the plant total exergy destruction rate and specific fuel consumption dropped by 10.8% and 7.0% respectively. The stack flue gas exit temperature reduced from 126°C to 84°C in the absorption refrigerator, thus reducing the environmental thermal pollution. The COP and exergy efficiency of the refrigeration cycle was 0.60 and 27.0%, respectively. Results also show that the highest rate of exergy destruction in the combined cycle power plant occurred in the combustion chamber while the highest rate of exergy destruction in the absorption refrigeration cycle occurred in the evaporator followed by the absorber.

Keywords: Absorption refrigeration; combined cycle power plant; gas turbine power plant; steam turbine power plant; psychrometric processes; waste heat utilization.

Nomenclature

h	Specific enthalpy, kJ/kg
$\dot{P}$	Pumping power, kW
$\dot{W}$	Power output, MW
$\dot{W}_{net}$	Net power output, MW
c_p	Specific heat capacity at constant pressure, kJ/kgK
$\dot{m}$	Mass flow rate, kg/s
R	Gas constant, kJ/kgK
s	Specific entropy, kJ/kgK
P	Pressure, Bar
T	Temperature, °C or K

Greek Letters

β	Number of gas turbine units
Δ	Change between states
η	Efficiency
γ	Specific heat ratio
ω	Specific humidity, kg/kg $_{da}$
ξ	Concentration by mass of LiBr in LiBr_H_2O solution

Subscripts and Superscripts

a	Air
a, v	Average
c	Compressor
cc	Combustion chamber
$cond$	Condenser
$cycle$	Thermodynamic cycle
da	Dry air
f	Fuel
g	Flue gas
gt	Gas turbine
i	Constituent or component
p	Pump
s	Steam
st	Steam turbine
t	Turbine
tot	Total
w	Water
wv	Water vapor

Abbreviations

el. Gen	Electric generator
AC	Air compressor
ACC	Air cooling coil
ARS	Absorption refrigeration system
CC	Combustion chamber
CCPP	Combined cycle power plant
COND	Condenser
COP	Coefficient of performance
GT	Gas turbine
HP	High pressure
HPFWP	High pressure feed water pump
HPST	High pressure steam turbine
HPHRSG	High pressure heat recovery steam generator
LHV	Lower heating value

LP	Low pressure
LPFWP	Low pressure feed water pump
LPHRSG	Low pressure heat recovery steam generator
LPST	Low pressure steam turbine
RH	Relative humidity
SC	Steam condenser
SH	Sensible enthalpy (or heat) change
SH_f	Sensible heat gain of fuel

1. Introduction

Globally, the current interest is on cost-effective and environment-friendly technologies for thermal power generation (fossil fuel-to-electric energy conversion). Due to its comparatively high efficiency and low exhaust temperature, the combined cycle power plant (CCPP) is now preferred to single cycle power plant. However, the power capability of a CCPP is significantly affected by the ambient temperature (Chuang & Sue 2005). For CCPP operating with air-cooled condenser, the ambient air conditions have direct impact on the performance of both the gas- and steam-turbine cycles (Bustamante et al. 2015). The gas turbine is designed to operate with a constant air volume flow in the compressor and normally at inlet air temperature of 15°C ISO condition (Al-ibrahim & Varnham 2010). When the inlet ambient air temperature increases, its specific volume increases, so that the mass flow rate entering the turbine is accordingly decreased, leading to decrease in the power output of the gas turbine (Zaki et al. 2011). Thus, the power output is dependent on the mass flow rate of the air in the plant. For each degree Celsius increase of the air temperature, the power outputs of the gas turbine and the combined cycles are reduced by 0.5–0.9% and 0.27%, respectively (Hosseini et al. 2007).

The performance and power output of the gas turbine power plant strongly depend on the compressor inlet air temperature (Singh 2016; Ameri & Hejazi 2004). Different inlet air cooling technologies are available for improving gas turbine cycle power output. They can be classified into two main categories: water evaporation systems and heat transfer systems. In water evaporation systems, a certain amount of demineralized water is sprayed into the inlet air stream, which evaporates, thus decreasing the air temperature. These include evaporative cooling, inlet fogging/air washing, and over-spray systems. According to Ehyaei et al. (2015), the minimum achievable temperature with these systems is limited to the ambient wet bulb temperature. In heat transfer systems, the coolant and the air stream do not come into contact; the inlet air cooling involves the use of mechanical chillers, absorption chillers or cold thermal storage systems. Lower air temperatures and therefore larger power outputs can be attained by the heat transfer systems based on refrigeration systems (Dawoud et al. 2005). Barigozzi et al. (2015) conducted techno-economic analysis of gas turbine inlet air cooling of CCPPs operating in three different climatic conditions. The system was based on cold water thermal storage charged by mechanical chillers. Their results showed that the best techno-economic performance of the inlet air cooling application was obtained from sites with high ambient temperatures and low relative humidity characterized by high net present values and low pay back time on investment, while wet climates required

larger cold storage thus increasing the investment costs. Relative humidity was shown to have a strong influence on the sizing of the cold storage tank.

Najjar & Abubaker (2015) performed thermo-economic analysis of a new form of gas turbine inlet air cooling system, called the indirect evaporative cooling system (IECS), which was combination of an air humidifier with a vapor compression mechanical chiller or absorption chiller for cooling part of the total air. Their results showed that with combined IECS and mechanical chiller, the power output and thermal efficiency of the gas turbine plant increased by 4% and 2%, respectively in hot and humid weather, while with combined IECS and absorption chiller, the power output and thermal efficiency increased by 11.9% and 9.8%, respectively, in hot and humid weather. The thermo-economic evaluation showed that although the capital cost for the combined IECS and absorption chiller system was the highest, it had the lowest payback period of 1 year, while the payback period for the combined IECS and mechanical chiller was 8 years.

Cooling the turbine inlet air can increase the power output substantially. This is because the specific volume of cooled air is smaller, giving the turbine a higher mass flow rate and resulting in increased turbine power output and cycle efficiency (Ameri & Hejazi 2004). A review by Al-ibrahim & Varnham (2010) shows that there are three main inlet air cooling methods: evaporative cooling using evaporative media or water spraying to the inlet air (fogging); cooling by the use of thermal energy storage, chilled water storage or ice harvesting; and cooling the inlet air by the use of refrigeration plant (vapor compression or absorption refrigeration). These techniques have been studied extensively, and are being applied to gas turbine plants around the world. Dawoud et al. (2005) compared these technologies with respect to their effectiveness in power boosting of small-size gas-turbine power plants used in two locations at Marmul and Fahud in Oman. Their findings showed that compressor inlet air cooling by fogging generated 11.4% more electric power in comparison to evaporative cooling in both locations. The aqua-lithium bromide absorption cooling produced 40% and 55% more electric power than cooling by fogging at Fahud and Marmul, respectively. Alhazmy & Najjar (2004) compared the use of two different types of air coolers, namely, water spraying system and cooling coil, to improve the performance of gas turbine power plants. Their results show that the water spray (evaporative) coolers operate efficiently in hot and dry climatic conditions, while the cooler coils (typical refrigeration systems) are better suited for use in humid climates. According to Boonnasa et al. (2006) the addition of absorption chiller to a CCPP for compressor inlet air cooling could increase the power output of a gas turbine by about 10.6% and the CCPP by around 6.24% annually. Mohapatra (2014) compared the impacts of integrating vapor compression and vapor absorption cooling system to a CCPP for inlet air cooling. Their study showed that the vapor compression inlet air cooling improved the specific power output by 9.02% compared to 6.09% obtained with the vapor absorption cooling. However, to operate the vapor compression system, power is extracted from the gas turbine output.

Due to the increasing focus on water conservation and the environmental effects of both once- through and evaporative cooling, the use of air-cooled condensers for rejecting heat in combined cycle power plant is increasing (Yang et al. 2012). In CCPPs with air-cooled condensers, heat is rejected directly or indirectly to the ambient air during the condensation

process. A drawback of the air-cooled condensers is that their performance can decline as ambient temperatures increase, which reduces the steam turbine power output. Increased ambient temperature reduces the heat transfer (heat rejection) rate during steam condensation leading to rise in turbine back pressure. As the turbine back pressure increases, the output of the steam turbine decreases (Ramani et al. 2011). Since air-cooled condensers operate with the ambient dry bulb temperature as the theoretical minimum attainable temperature, their efficiency can drop by about 10% when ambient temperatures rise (Gadhamshetty et al. 2006; Nirmalakhandan et al. 2008). A field performance test reported by Chuang & Sue (2005) on an active CCPP with air-cooled condenser showed that CCPP could produce more power output when operating at a lower ambient temperature (or lower condenser pressure); for each 1^{o}C drop in ambient temperature, the power output of the CCPP increased by 0.6% and efficiency improved by 0.1%.

Some approaches have been used or proposed to maintain air-cooled condenser performance under higher ambient temperatures. The first approach (the most popular) is to increase the turbine exhaust pressure whereby the condensing temperature is increased. This results in a reduction in net power output of the steam turbine. The second approach is to increase the air flow through the air-cooled condenser during the hot period. This approach entails additional energy consumption and over-sizing of the fans. The third approach is to cool the air-cooled condenser intake air by spraying water. This system requires makeup water and hence, no longer qualifies as a "true" dry cooled system. Incomplete evaporation of water droplets may increase the risk of corrosion, scaling and environmental discharge violations (Gadhamshetty et al. 2006; Nirmalakhandan et al. 2008). In the fourth approach (Gadhamshetty et al. 2006; Nirmalakhandan et al. 2008), a sensible heat, low temperature thermal energy storage (TES) system is used to pre-cool the ambient air supply to the air compressor (AC) and the air-cooled condenser. The TES system is maintained at the specified temperature by a LiBr-H2O absorption refrigeration system (ARS) driven by waste heat from the stack gases of the CCPP. A major concern with the TES is the large volume of the storage tank, which is a function of plant capacity as well as the design inlet air temperature to the air-cooled condenser. However, both research based their studies on energy analysis of combined cycle plants operating in the arid regions and not in the hot and humid regions. In wet cooling systems, the effectiveness of the evaporative cooling process, is influenced by the relative humidity of the ambient air at the specific location, the higher the relative humidity, the lower the rate of cooling by evaporation (Ataei et al. 2008).

Thus, in hot and humid regions such as Southern Nigeria, latitude 4°45′N and longitude 7°00′E, where the annual average relative humidity is about 80% (Oko & Ogoloma 2011), power plants with air-cooled condensers are increasing in number. Singh (2016) performed exergy and energy analysis of an active combined cycle power plant using exhaust heat operated ammonia-water absorption refrigeration system for inlet air cooling. Based on the Indian climatic conditions, the results showed that the power output, energy and exergy efficiencies of the plant increased by 9440kW, 1.193% and 1.133% respectively, during the summer season, while the power output increased by 400kW during the winter season. However, this study did not consider the effect of cooling the steam condenser. Therefore, the main aim of this paper is to present an energy and exergy based performance analysis of

an existing CCPP retrofitted with a waste heat driven aqua lithium bromide absorption refrigerator for cooling inlet air streams to the compressor and air-cooled steam condenser. The active CCPP operates in the tropical rain forest region of Southern Nigeria at latitude 4°45′N and longitude 7°00′E. Parametric variations were considered to determine the impact of ambient conditions on the performance of the combined cycle power plant. A chilled water circulation arrangement to reduce the volume requirement of the chilled water was considered. It is expected that the results of this study will encourage operators of combined cycle power plants in hot and humid regions such as Nigeria, to make appropriate modifications to their plants for performance improvement. The results and simulations were generated using the MATLAB and Engineering Equation (EES) software.

2. Problem Formulation and Solution Methods

The system diagrams, principles of operation and the thermodynamic modeling of the existing power plant and absorption refrigeration system are presented in this section.

2.1 System description

The proposed system is made up of the gas-turbine cycle (GTC) unit, the steam-turbine cycle unit (STC), and the absorption refrigeration cycle unit (ARC). The first two units are the existing gas and steam CCPPs, which are to be retrofitted to include a waste-heat-driven H_2O-LiBr absorption refrigerator to provide all the cooling load required by the power plant, Figure 1.

The CCPP consists of: three natural gas fired gas turbine (GT) units; three dual pressure, forced circulation heat recovery steam generators (HRSG); a dual pressure steam turbine (ST) unit. The phase diagram of the CCPP is shown in Figure 2. Inlet air at the ambient temperature (state 1) is compressed by the AC to state 2 before entering the combustion chamber (CC) where it mixes and reacts with the natural gas from the fuel supply system to produce hot flue gases, which exit the CC and enter the GT. The flue gases expand in the GT from state 3 to state 4, producing power for driving the AC and for conversion into electricity in the electric generator (el. Gen1).

The exhaust flue gases at state 4 pass through the HRSG where high- and low-pressure (HP and LP) feed water streams are heated to states 7 and 9, respectively, as the flue gases exit the HPHRSG and LPHRSG at states 5 and 6, respectively. The superheated steam from the HPHRSG at state 7 expands in the high pressure turbine (HPST) to state 8, and mixes with the superheated steam from the LPHRSG at state 9 to form a homogenous steam mixture at state 10 before expanding in the low pressure steam turbine (LPST) to state 11. The mechanical power from the steam turbines is converted into electrical power in the electrical generator 2 (el. Gen 2). The exit wet steam is condensed in the air-cooled steam condenser (SC) to saturated liquid water at state 12 before being pumped by the low pressure feed water pump (LPFWP) to state 13. One part of this low pressure feed water ($\alpha\dot{m}$) is fed into the LPHRSG, while the remaining part ($(1-\alpha)\dot{m}$) is pumped by the high pressure water pump (HPFWP) to state 14 and fed into the HPRSG for the dual-pressure steam turbine cyclic process to continue repeating.

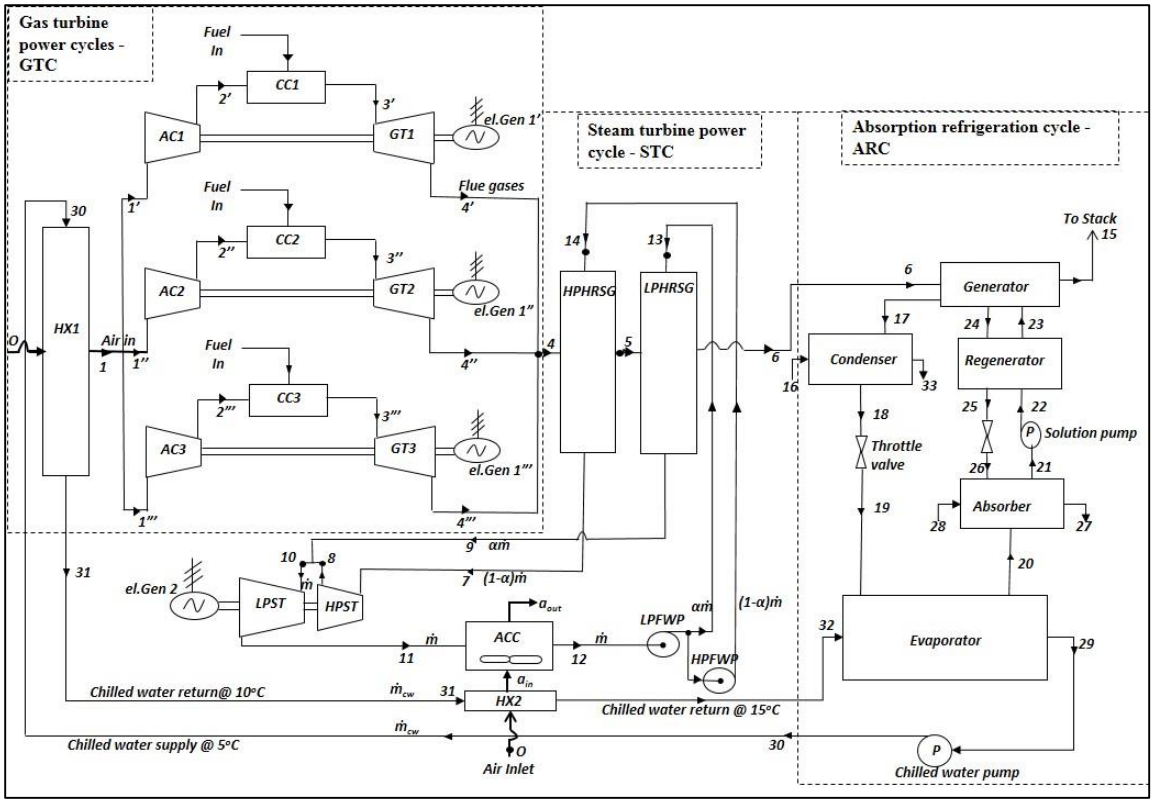

Figure 1. Plant diagram of the proposed thermal power and refrigeration plant.

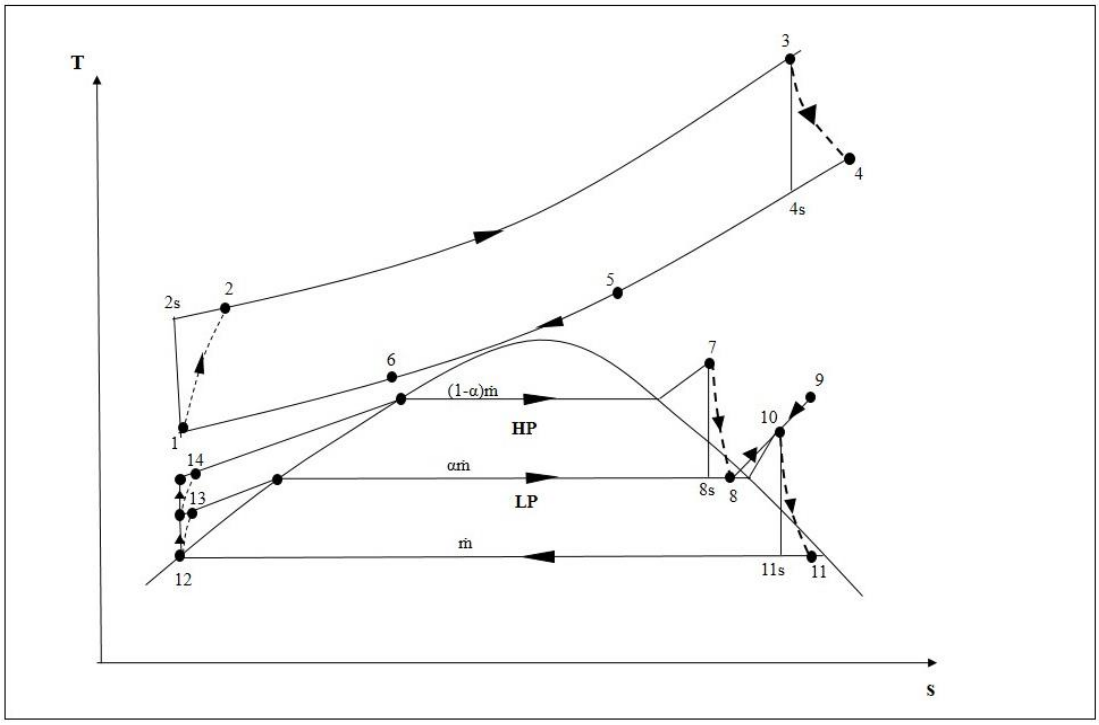

Figure 2. T-s diagram of the combined power cycle showing the relevant thermodynamic processes in the gas- and steam-turbine cycles.

At state 6, the exhaust flue gases exiting the HRSG units are used to power the LiBr-H_2O absorption refrigeration unit (ARC) and then discharged at state 15 into the atmosphere. The ARC consists of a generator, regenerator, absorber, condenser, evaporator, solution feed pump and two expansion valves. Dilute LiBr-H2O solution in the absorber is pumped from state 21 through the regenerator to the generator at 23. In the refrigerant generator, the diluted solution is heated directly by the exhaust gases. A large portion of water in the LiBr-H_2O solution is evaporated. The generated pure water vapor enters the refrigerant condenser, while the concentrated LiBr–H_2O solution at state 24 returns to the absorber through the regenerator (state 25) and throttle valve (state 26). The evaporated refrigerant (water) vapor at state 17 is condensed as it passes through the condenser to state 18, throttled to low pressure and temperature to state 19, before entering the evaporator, where it is evaporated by the heat from the circulating water from the air cooling coils to state 20. The saturated refrigerant vapor from the evaporator at state 20 enters the absorber, where it is absorbed by the concentrated solution from the generator at state 26. The resulting diluted solution at state 20 is pumped to the generator through the regenerator to complete the absorption refrigeration cycle.

Chilled water pump circulates chilled water at 5°C from the evaporator (state 29) through an air cooler / heat exchanger (HX1) to cool the inlet air (state 1) to the ACs. During this heat exchange process, the temperature of chilled water increases to 10°C. The same volume of chilled water (now at 10°C) flows from state 31 through another air cooler (HX2) to cool the inlet air (a_{in}) to the air-cooled steam condenser (ACC); gaining more heat to reach 15°C. Finally, the chilled water returns to the evaporator where it is cooled to 5°C by the ARC and the cycle continues repeating. As the inlet air stream is cooled from the given ambient conditions at the plant location, the air temperature drops while the relative humidity gradually rises, as shown Figure 3.

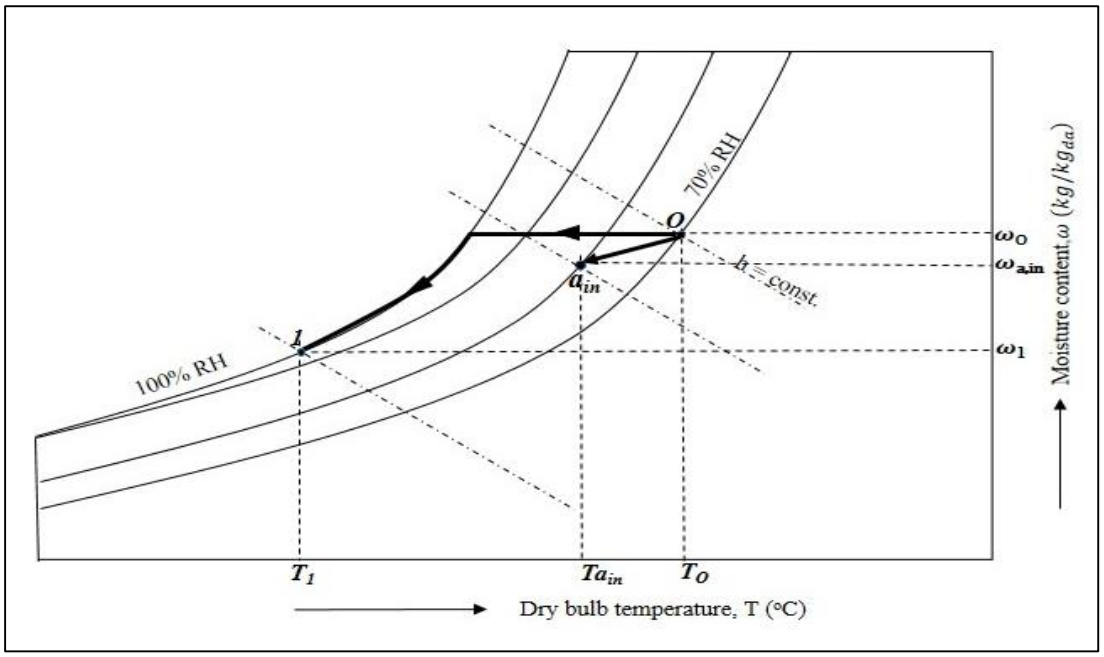

Figure 3. Psychrometric chart of the compressor and steam condenser inlet air cooling processes.

2.2 Assumptions for the thermodynamic modeling

The following assumptions were made in performing the energy and exergy analysis of the gas turbine cycle , the steam turbine cycle and the LiBr – H_2O absorption refrigeration cycle:

- Mass and energy flow through the plant are in steady state.
- Changes in kinetic and potential forms of energy are negligibly small.
- All gases (air and flue gases) behave like ideal gases.
- Heat losses and mechanical losses were neglected.
- Air and water enter the system at ambient temperature and pressure.
- The thermodynamic equations are derived for the major thermodynamic devices by treating them as control volumes.
- The mass flow rates and thermodynamic characteristics of the three gas turbine units are identical, so that only one is analyzed and the extensive outputs are multiplied by a factor of 3.
- Solution leaving the absorber and the generator are assumed to be saturated and in equilibrium conditions at their operating temperatures and concentrations.
- The refrigerant states leaving the condenser and evaporator are also assumed to be saturated
- The environmental dead/reference state conditions are $P_o = 101.325$kPa and $T_o = 303$K.

2.3 Thermodynamic analysis of the combined cycle power and refrigeration plant

2.3.1 Energy and exergy analysis of the existing gas- and steam-turbine power cycles

The major units of the CCPP undergo different thermodynamic processes (Figure 2). The energy analysis based on First Law of Thermodynamics cannot be used to determine the sources of irreversibilities in a system. But the exergy analysis can determine the magnitudes, locations and causes of irreversibilities in the plants, and also provide more meaningful assessment of plant individual components' efficiencies (Ahmadi et al. 2013; Ameri & Enadi 2012). The general steady state, steady flow energy equation for a control volume (cv) is given as (Bejan, A., Tsatsaronis, G., and Moran, M. 1996):

$$\dot{Q}_{cv} - \dot{W}_{cv} + \sum_j \dot{m}_i h_i - \sum_j \dot{m}_e h_e = 0 \quad (1)$$

where, $\dot{Q}_{cv}$, $\dot{W}(kW)$, $\dot{m}$ (kg/s) and h (kJ/kg) are the rates of heat interaction, power output and mass flow and specific enthalpy respectively; the subscripts i and e mean inlet and exit, respectively; and the subscript j denotes the jth portion of the control surface. The energy efficiency is a measure of the useful energy from a system to the input energy into the system. The energy efficiencies of different systems are defined following the convention. For the thermal power plant, the cycle thermal efficiency is given as:

$$\eta_{th} = \frac{\dot{W}_{net}}{\dot{Q}_h} = 1 - \frac{\dot{Q}_{R,CCPP}}{\dot{Q}_h} \quad (2a)$$

where, $\dot{W}_{net}$, $\dot{Q}_h$ and $\dot{Q}_{R,CCPP}$ (kW) are the net power, rates of heat addition and rejection in the cycle respectively. The rates of heat addition in the combustion chamber,$\dot{Q}_{cc} = \dot{Q}_h$, and heat rejection in the HRSG, state 6,$\dot{Q}_{R,CCPP}$, are respectively given as (Zaki et al. 2011):

$$\dot{Q}_h = \dot{m}_f[\eta_{cc}\, LHV + SH_f] = \dot{m}_f[\eta_{cc}\, LHV + c_{pf}\,(T_f - T_i)] \quad (2b)$$

and

$$\dot{Q}_{R,CCPP} = \dot{Q}_h - \dot{W}_{net,CCP} \quad (2c)$$

where, $\dot{m}_f$ (kg/s) is the fuel mass flow rate; η_{cc} $(-)$ is the combustion efficiency and accounts for the incomplete combustion and heat losses in the combustion chamber; LHV (kJ/kg) is the lower heating value of the fuel gas at the initial temperature; SH_f (kJ/kg) is the increase in sensible enthalpy of the fuel gas due to preheating before entry to combustion chamber; T_i (K) is the fuel gas initial temperature before preheating; T_f (K) is the temperature of gas after preheating /entry to combustion chamber; c_{pf} (kJ/kg.K) is the specific heat capacity of the fuel (natural gas); and $\dot{W}_{net,CCP}$ (kW) is the net power output of the CCPP given as:

$$\dot{W}_{net,CCP} = \dot{W}_{net,GTC} + \dot{W}_{net,STC} \quad (2d)$$

Exergy destruction is an important parameter in the analysis of energy devices and is defined as the potential work lost due to irreversibility (Al-sulaiman et al. 2012). The exergy destruction rate of a steady state, steady flow control volume is given as (Oko & Njoku 2017; Talbi & Agnew 2000; Touaibi et al. 2013; Ahmadi et al. 2012; Khaliq 2009):

$$\dot{E}x_{D,cv} = \sum_j \left(1 - \frac{T_o}{T_j}\right)\dot{Q}_j - \dot{W}_{CV} + \sum \dot{m}ex_i - \sum \dot{m}ex_e \quad (3)$$

where, $\dot{E}x_D$ (kW) and ex (kJ/kg) are the rate of exergy destruction and specific exergy, respectively; and the subscript o denotes the reference environment (the dead state). Exergy efficiency is a measure of the exergy output from a system or device to the exergy input into the system or device; for thermal power cycle, it can be expressed as (Ahmadi et al. 2013; Ahmadi et al. 2012; Ersayin & Ozgener 2015):

$$\eta_{II} = \frac{\dot{W}_{net}}{\Delta\dot{G}_o} = 1 - \frac{\dot{E}x_{d,cycle}}{\Delta\dot{G}_o} \quad (4)$$

$$\Delta\dot{G}_o = \dot{m}_f \times \phi \times LHV \quad (5)$$

where, $\Delta\dot{G}_o$ (kW) is the fuel exergy rate; ϕ is the ratio of fuel chemical exergy to the lower heating value (LHV), $\phi = 1.06$ for natural gas (Nag 2013). Further details on the models used for the energy and exergy analysis of the gas turbine cycle, steam turbine cycle and the combined cycle power plant in this study are presented in the authors' previous study (Oko & Njoku 2017).

2.3.2 Energy and exergy analysis of the LiBr-H2O absorption refrigeration cycle (ARC)

Following some previous works (Dinçer et al. 2018; Dincer & Ratlamwala 2016; Popli et al. 2013; Touaibi et al. 2013; Kaushik & Arora 2009; Muhsin & Kaynakli 2007), the ARC is analyzed based on Figures 1 and 2, as follows:

Refrigerant generator:

Energy balance across the generator is given as:

$$\dot{Q}_{gen} = \dot{m}_{rf} h_{17} + \dot{m}_{ws} h_{24} - \dot{m}_{ss} h_{23} = k\dot{m}_g c_{pg} (T_6 - T_{15}) \quad (6a)$$

where, k is the number of turbines in the gas turbine power unit, in this case,$k = 3$;$\dot{m}_{rf}$,$\dot{m}_{ws}$, $\dot{m}_{ss}$ and $\dot{m}_g$(kg/s) are the mass flow rates of the refrigerant (water vapor evaporated in the generator), weak solution, strong solution, and flue gases, respectively. The rate of exergy destruction in the refrigerant generator is given as:

$$\dot{E}x_{D,gen} = \left(1 - \frac{T_o}{T_g}\right) \dot{Q}_{gen} - \left(\dot{E}x_{24} - \dot{E}x_{23} + \dot{E}x_{17}\right) \quad (6b)$$

Refrigerant condenser:

The rate of heat rejected in the condenser where saturated water vapor (refrigerant) from the generator is cooled to saturated liquid at the generator pressure is given as:

$$\dot{Q}_{cond} = \dot{m}_{rf} (h_{17} - h_{18}) \quad (7a)$$

The rate of exergy destruction in the condenser is given as:

$$\dot{E}x_{D,cond} = \left(\dot{E}x_{17} - \dot{E}x_{18}\right) - \left(1 - \frac{T_o}{T_{cond}}\right) \dot{Q}_{cond} \quad (7b)$$

where, T_{cond} (K) is the temperature in the refrigerant condenser.

Throttle valves:

The pressure of liquid refrigerant at generator pressure is reduced isenthalpically to the evaporator pressure, $h_{18} = h_{19}$ and $h_{25} = h_{26}$; so that the rates of exergy destruction in the solution and refrigerant throttle valves respectively are:

$$\dot{E}x_{D,STV} = T_0 \dot{m}_{ws} (s_{26} - s_{25}) \quad (8a)$$

and

$$\dot{E}x_{D,RTV} = T_0 \dot{m}_{rf} (s_{19} - s_{18}) \quad (8b)$$

Refrigerant evaporator:

The liquid refrigerant at low pressure is evaporated by the circulating chilled water used for inlet air cooling in the air cooling coil (ACC), and becomes saturated vapor. The refrigeration (or cooling) load, $\dot{Q}_{CL}$ (kW), is given as:

$$\dot{Q}_{Evap} = \dot{m}_{rf}(h_{20} - h_{19}) = \dot{Q}_{CL} \quad (9a)$$

The rate of exergy destruction in the evaporator is given as:

$$\dot{E}x_{D,Evap} = \left(\frac{T_e}{T_o} - 1\right)\dot{Q}_{evap} - \left(\dot{E}x_{20} - \dot{E}x_{19}\right) \quad (9b)$$

Refrigerant absorber:

In the absorber, the weak solution from the generator which has been throttled to the absorber pressure readily absorbs the saturated refrigerant vapor from the evaporator to become a strong solution. This exothermic process releases some heat, which is removed by the cooling fluid flowing through the absorber. The rate of heat rejection from the absorber is given as:

$$\dot{Q}_{abs} = (\dot{m}_{rf}h_{20} + \dot{m}_{ws}h_{26}) - (\dot{m}_{ss}h_{21}) = \dot{m}_{abs}(h_{27} - h_{28}) \quad (10a)$$

where, $\dot{m}_{abs}$ (kg/s) is the mass flow rate of the cooling fluid in the absorber. The rate of exergy destruction in the absorber is given as:

$$\dot{E}x_{D,abs} = \left(\dot{E}x_{21} - \dot{E}x_{26} - \dot{E}x_{20}\right) - \left(1 - \frac{T_o}{T_{abs}}\right)\dot{Q}_{abs} \quad (10b)$$

where, T_{abs} (K) is the temperature in the absorber.

Solution pump:

The pump transfers the strong LiBr-H_2O solution from the absorber to the generator, and its power consumption, which is usually negligibly small, is given as:

$$\dot{W}_{sp} = \dot{m}_{ss}(h_{22} - h_{21}) \quad (11a)$$

The rate of exergy destruction in the solution pump is given as:

$$\dot{E}x_{D,sp} = T_0\dot{m}_{ss}(s_{22} - s_{21}) \quad (11b)$$

Regenerator:

The regenerator heats the strong solution from the absorber on its way to the generator and cools the weak solution returning from the generator to the absorber. The regenerator heat and exergy destruction rates respectively are:

$$\dot{Q}_{reg} = \dot{m}_{ws}(h_{24} - h_{25}) = \dot{m}_{ss}(h_{23} - h_{22}) \quad (12a)$$

and

$$\dot{E}x_{D,reg} = \left(\dot{E}x_{24} - \dot{E}x_{25}\right) - \left(\dot{E}x_{23} - \dot{E}x_{22}\right) \quad (12b)$$

Coefficient of performance of the absorption refrigeration cycle:

$$COP = \frac{\dot{Q}_{Evap}}{\dot{Q}_{gen}+\dot{W}_{sp}} \quad (13a)$$

Exergy efficiency of the absorption refrigeration cycle:

$$\eta_{II,ARS} = \frac{\dot{Q}_{Evap}\left(\frac{T_0}{T_e}-1\right)}{\dot{Q}_{gen}\left(1-\frac{T_0}{T_g}\right)+\dot{W}_{sp}} \quad (13b)$$

where, T_e and T_g (K) are the temperatures of the refrigerant in the evaporator and the logarithmic mean temperature of the waste flue gases in the refrigerant generator, respectively.

2.3.3 Inlet air cooling load analysis

The total cooling load comprises of the heat removed to reduce the ambient air temperature from its initial ambient condition to the desired cooled state, i.e. the sensible heat of air and the heat required to condense the moisture contained in the air (the latent heat). Thus, the total inlet air cooling load or the refrigerating capacity, $\dot{Q}_{CL}$ (kW), is the summation of both the sensible ($\dot{Q}_s$) and the latent ($\dot{Q}_L$) cooling loads:

$$\dot{Q}_{CL} = \dot{Q}_s + \dot{Q}_L = \dot{Q}_{Evap} \quad (14a)$$

The sensible cooling load can be determined as (Dawoud et al. 2005):

$$\dot{Q}_s = \frac{\dot{V}_a}{v_a} c_{pa}(T_0 - T_1) \quad (14b)$$

where, $\dot{V}_a$(m3/s) is volume flow rate of air based on actual data acquired from the plant; T_0(K) is the dry bulb temperature of the ambient air; and T_1 (K) is the cooled air temperature at state 1; v_a(m3/kg) is the specific volume of the humid air per kilogram of dry air. The specific volume of humid air per kilogram of dry air may be given as (Dawoud et al. 2005):

$$v_a = (0.287 + \omega_O\ 0.462)\frac{T}{P_{atm}} \quad (14c)$$

where, T (K) is the dry bulb temperature; P_{atm} (kPa) is the atmospheric pressure; $\omega_O(kg_{wv}/kg_{da})$ is the specific humidity of the air which is given by(Cengel & Boles 2011; Oko & Diemuodeke 2010):

$$\omega_O = \frac{0.622\ RH_O}{(P_{atm} - RH_O)}P_{wv} \quad (14d)$$

where, P_{wv} (kPa) is the saturation water vapor pressure at the given dry bulb temperature, T; $RH_O(-)$ is the relative humidity of the air. The latent cooling load, $\dot{Q}_L$ (kW), is given as:

$$\dot{Q}_L = \frac{\dot{V}_a}{v_a}\left[\omega_O\left(c_{pv}T_O + h_{fg}\right) - \omega_1\ (c_{pv}T_1 + h_{fg}) - (\omega_O - \omega_1)\ c_{pw}T_1\right] \quad (14e)$$

where, c_{pv} (kJ/kg. K) is the isobaric specific heat capacity of water vapor in the humid air; h_{fg} (kJ/kg) is the air latent heat of evaporation of water at 0oC; ω_1(kg/kg. da) is the specific humidity of the air at the desired compressor inlet temperature; and c_{pw}(kJ/kg. K) is the isobaric specific heat capacity of liquid water. The mass flow rate of chilled water circulating from the evaporator through the air coolers, $\dot{m}_{cw}$ (kg/s), is given as:

$$\dot{m}_{cw} = \frac{\dot{Q}_{CL}}{C_{pw}\,(T_{32} - T_{29})} \tag{15}$$

where, T_{29} is the chilled water supply temperature and T_{32} is the water return temperature. The pump power required for chilled water circulation ($\dot{W}_{cwr}$) is given as:

$$\dot{W}_{cwr} = \frac{\dot{m}_{cwr}\,\Delta P}{\rho} \tag{16}$$

where, ρ (kg/m3) is the density of water and ΔP (kPa) is the pressure loss to be overcome by the pump.

2.3.4 Data used for the generation of results

The operating log data of the active CCPP and other thermodynamic specifications used in this study are presented in Table 1.

Table 1. Input data for the analysis of the tricycle power and refrigeration plant

Plant unit	Parameter	Symbol	Unit	Value
Operating data of the existing CCPP[1]				
Compressor	Inlet temperature	T_O	oC	30
	Relative humidity of air	RH_O	%	70
	Inlet air pressure	P1	kPa	99
	Volume flow rate of air (×3)	V1	m3/s	1287
Combustion chamber	Inlet air pressure	P2	kPa	1380
	Fuel inlet temperature	T_f	oC	60.2
	Fuel inlet pressure	P_f	kPa	2650
	Fuel mass flow rate (×3)	$\dot{m}_f$	kg/s	25.83
	Fuel lower heating value	LHV	kJ /kg	52580
Gas turbine	Outlet temperature of flue gases	T4	oC	531
	Net power output (×3)	$\dot{W}_{net,GTC}$	MW	447
	Flue gas mass flow rate (×3)	$\dot{m}_g$	kg/s	1509.3
HRSG	Stack exhaust temperature	T6	oC	126
Steam turbine	Net power output	$\dot{W}_{net,STC}$	MW	202
	Inlet steam high pressure (HP)	P7	kPa	10020
	Inlet steam low pressure (LP)	P10	kPa	537
	Mass flow rate of HP steam	$\dot{m}_{SHP}$	kg/s	175.2
	Mass flow rate of LP steam	$\dot{m}_{SLP}$	kg/s	54.7
	Inlet temperature of HP steam	T7	oC	512
	Inlet temperature of LP steam	T10	oC	257.2
	Inlet wet steam temperature	T11	oC	60.7

Air-cooled condenser	Inlet saturated water pressure	P12	kPa	21
	Air mass flow rate	$\dot{m}_{ca}$	kg/s	160680
Other thermodynamic specifications	Combustion efficiency[2]	η_{CC}	–	0.98
	Flue gas constant	R_g	kJ/kgK	0.285
	Steam turbine isentropic efficiency[3]	$\eta_{s,ST}$	-	0.82
	Feed pump isentropic efficiency	$\eta_{s,FWP}$	-	0.90
	Desired compressor inlet air temp.[4]	T_1	°C	15
	Air relative humidity at cooling coil exit	RH_1	%	100
	Density of chilled water	ρ	kg/m^3	1000
	Pressure loss overcome by chilled water circulation pump	ΔP	kPa	9.8×10^5
	Chilled water supply temperature	T_{29}	°C	5
	Chilled water return temperature	T_{32}	°C	15

[1](Afam VI Combined Cycle Gas Turbine Plant (CCGT) 2015); [2](Saravanamuttoo et al. 1996); [3](Tiwari et al. 2013); [4](Boonnasa et al. 2006)

3. Results and Discussion

3.1 Validation of models for the existing CCPP

Using the fuel heat input rate of 1333MW and the fuel chemical exergy input rate of 1374MW, key performance characteristics of the existing combined cycle power plant were computed. The computed values were compared with their corresponding measured operating values of the active CCPP, as presented in Table 2. The error margins were within the acceptable range for power plant applications.

Table 2. Comparison of measured and computed characteristics of the existing CCPP

Parameter	Measured data	Computed value	Error (%)
Gas turbine net power output (MW)	447.0	441.3	1.28
Gas turbine exit temperature (°C)	531.3	527.5	0.72
Gas turbine outlet mass flow (kg/s)	1509.3	1476.3	2.19
Steam turbine power output (MW)	202.3	200.2	1.04
HRSG exit flue gases temperature (°C)	126.0	123.9	1.67

3.1 Thermodynamic characteristics of the combined power plant and absorption refrigeration system

The computed key performance parameters of the gas turbine cycle, steam turbine cycle and the combined cycle power plants with and without inlet air cooling are tabulated in Table 3. It clearly shows that by cooling the inlet air to the compressors to 15°C, the net power output of the gas turbine cycle is increased by 48.3MW, and by cooling the inlet air streams to the air-cooled steam condenser to 29°C, the net power output of the steam turbine cycle is increased by 1.4MW. Cumulatively, the compressor and condenser inlet air cooling could increase the net power of the CCPP by 7.7%. This result is higher than that reported in

previous studies (Boonnasa et al. 2006; Mohapatra 2014) because these studies only considered compressor inlet air cooling but did not consider steam condenser cooling. Furthermore, the overall thermal and exergy efficiencies of the CCPP is increased by 8.1% and 7.5%, respectively. The overall rate of exergy destruction and specific fuel consumption are decreased by 10.8% and 7.0% respectively. The stack discharge temperature of the exhaust flue gases after passing through the absorption refrigeration unit is determined to be 84°C.The exergy analysis of the existing combined cycle power plant indicated that the highest rate of exergy destruction (about 59%) occurs in the combustion chamber of GT plant. The distribution of the percentage exergy destruction in the CCPP (Figure 4) closely agrees with the work of Ersayin & Ozgener (2015). The key input and computed parameters of the absorption refrigeration system are presented in Table 4. The low coefficient of performance (COP) of the absorption refrigeration cycle under consideration is due to its high temperature difference between generator T_{gen} (K) and evaporator temperature, T_e (K) as may readily be verified from the equivalent Carnot COP, $(T_{gen} - T_e)/[T_{gen}(T_0 - T_e)]$.

Table 3. Comparison of power plant performance parameters with and without inlet air cooling

Performance parameter	Gas turbine cycle	Steam turbine cycle	Combined cycle	Net change in CCPP (%)
Net power output (MW)				
Without inlet air cooling	441.3	200.0	641.3	--
With compressor and condenser inlet air cooling	489.6	201.4	691.0	7.7
Exergy destruction rate (MW)				
Without inlet air cooling	504.7	150.4	655.1	--
With compressor and condenser inlet air cooling	421.6	162.5	584.1	-10.8
Thermal efficiency (%)				
Without inlet air cooling	33.1	28.6	48.1	-
With compressor and condenser inlet air cooling	37.1	28.8	52.0	8.1
Exergy efficiency (%)				
Without inlet air cooling	32.1	28.1	46.7	--
With compressor and condenser inlet air cooling	36.0	26.7	50.2	7.5
Specific fuel consumption (kg/MWh)				
Without inlet air cooling	210.8	--	48.3	--
With compressor and condenser inlet air cooling	189.9	--	44.9	-7.0

The exergy destruction rates in the components of the LiBr-H_2O absorption refrigeration system are shown in Figure 5. It can be observed that the highest rate of exergy destruction occurs evaporator followed by the absorber relative to the other components. This may be due to the irreversibilities associated with the phase change and high temperature difference between the refrigerated water and evaporator space in the evaporator, and the mixing and heat transfer processes occurring in the absorber. A similar trend was observed in the work of Dinçer et al.(2018) for single effect absorption refrigeration chiller.

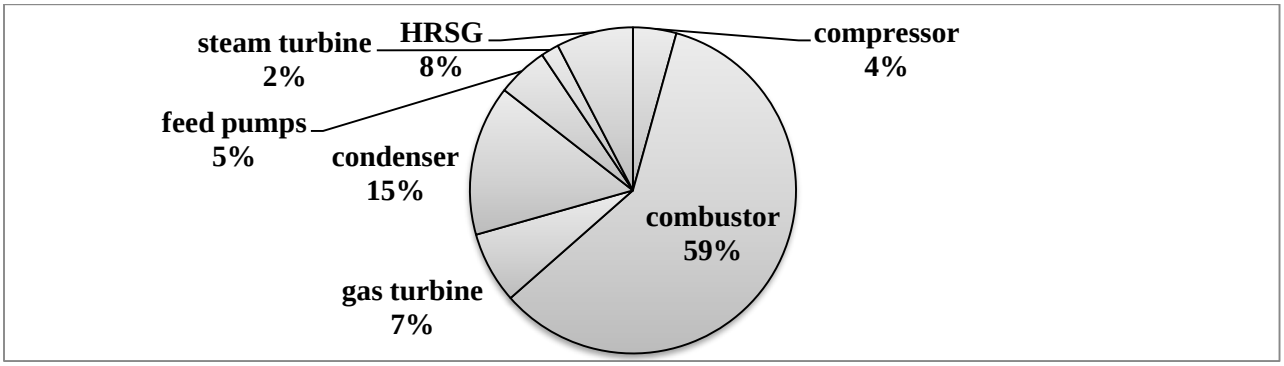

Figure 4. Exergy destruction distribution in CCPP.

Table 4. LiBr-H_2O absorption refrigeration system parameters

Parameter	Value
Generator temperature, T_{gen} (°C)	95.0
Condenser temperature, T_{cond} (°C)	46.0
Absorber temperature, T_{abs} (°C)	30.0
Evaporator temperature, T_e (°C)	5.0
Input thermal energy (MW)	74.6
Total cooling load (MW)	44.4
Total exergy destruction rate (MW)	31.8
Coefficient of performance, COP (-)	0.60
Exergy efficiency, $\eta_{II\,ARS}$ (%)	27.0

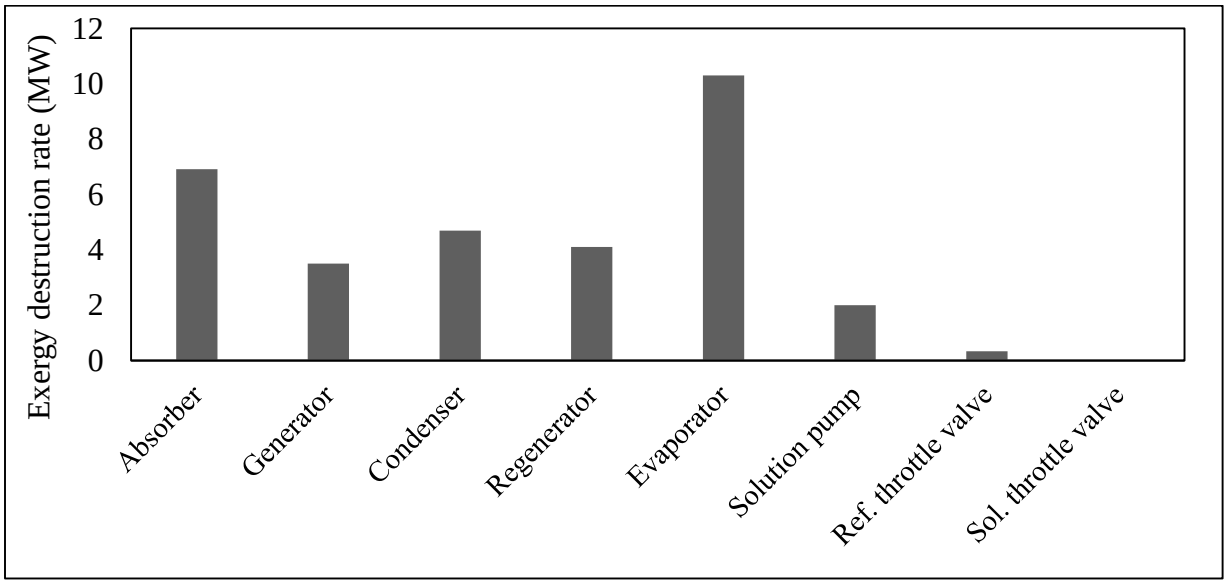

Figure 5. Rates of exergy destruction distribution in the absorption refrigeration system.

3.2 Sensitivity tests of some key parameters

The influence of variations in ambient air conditions on combined cycle plant performance has been analyzed and performance curves generated by varying various parameters. Figures 6 and 7 highlight the effects of variations in ambient air temperature and relative humidity on gas turbine and combined plant performance. An increase in either temperature or relative humidity results in reduced power output and increase in the rates of exergy destruction within the power plants. As the density of air is inversely proportional to the temperature, the increase in air temperature results in decrease of the air density and thus lower air mass flow rate, since the volume flow rate is constant. Consequently, the net power output decreases These results are in agreement with previously published results (Hosseini et al. 2007; Popli et al. 2013; Mohapatra 2014).

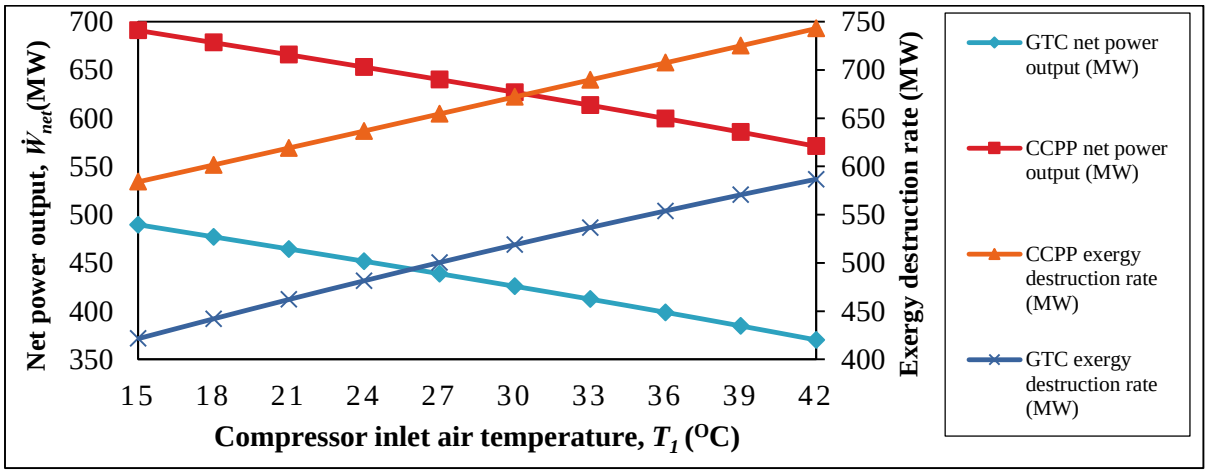

Figure 6. Effect of compressor inlet air temperature on the gas turbine-and combined cycle net power outputs.

As inlet air relative humidity increases (at constant fuel flow rate into the combustion chamber), the combustion temperature and the turbine inlet temperature decreases due to the presence of water vapor which absorbs some part of the heat of combustion (Jonsson & Yan 2005), resulting in drop in turbine output as shown in Figure 7. Figure 8 shows that, as compressor inlet air temperature increased, the thermal and exergy efficiencies of the gas turbine cycle and combined cycle power plants dropped while the specific fuel consumptions increased. Similar trend was reported in the reference (Memon et al. 2013). Figure 9 indicates that ambient air temperature has significant impact on the performance of an air-cooled steam condenser and power output of the steam turbine cycle. As the condenser cooling air temperature increased, the steam turbine cycle power output dropped, and the energy and exergy efficiencies of the steam turbine cycle and combined cycle power plants dropped respectively. Thus, the performances of steam turbine cycle and combined cycle power plants fitted with air-cooled steam condensers, could be improved by lowering the temperature of the cooling air streams. This is in line with previous works (Gadhamshetty et al. 2006; Nirmalakhandan et al. 2008; Chuang & Sue 2005).

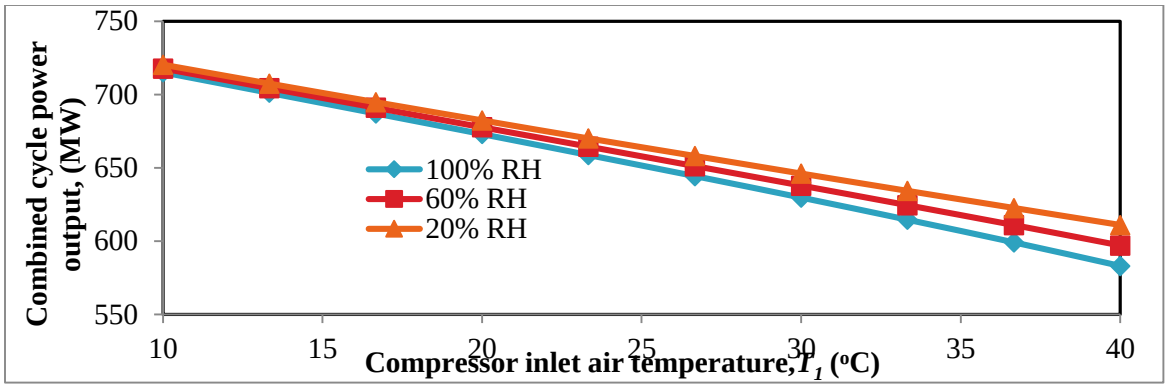

Figure 7. Effects of varying ambient temperature and relative humidity on the CCPP power output.

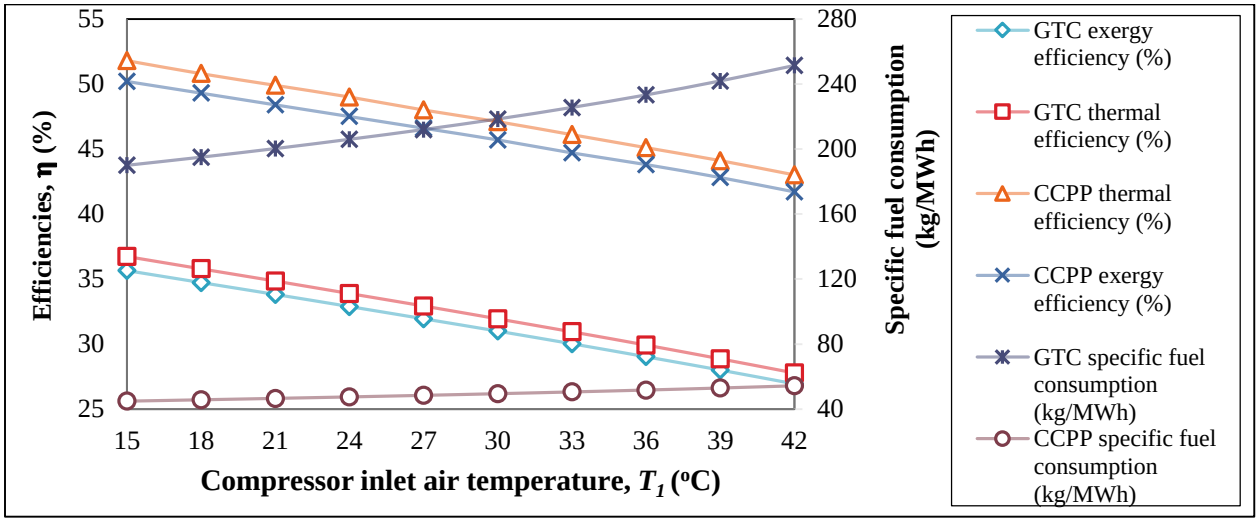

Figure 8. Variations of the gas turbine cycle and combined cycle power plant efficiencies, and specific fuel consumption, SFC (kg/MWh), with ambient inlet air temperature, T_1.

Since the primary heat input to CCPP and refrigeration unit was generated in the combustion chamber, the effects of variations in the combustion efficiency on the performance of the gas turbine cycle and combined cycle power plants were investigated. Figure 10 shows the effects of varying combustion efficiency on the net power outputs of the gas turbine and combined cycle power plants, and on the exit temperature of the flue gases leaving the HRSG. It can be observed that as combustion efficiency increases the net power outputs of the GTC and combined cycle power plants increase, and the temperature of the flue gases leaving the HRSG increases, leading to increase in the grade of heat input to the adjoining absorption refrigeration unit (ARC).

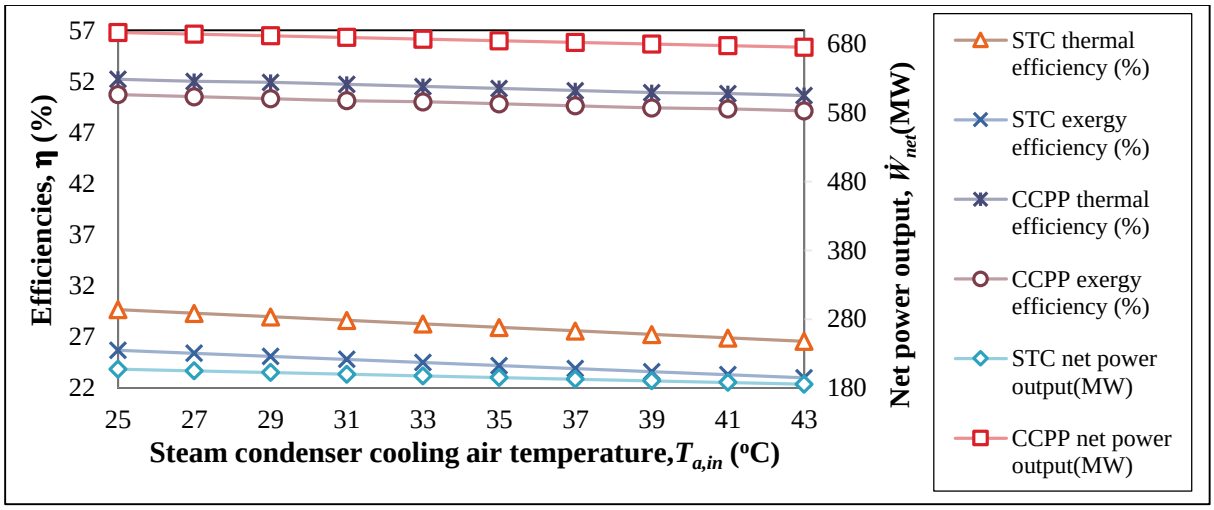

Figure 9. Steam condenser cooling air temperature versus steam turbine, combined cycle plant power output, energy and exergy efficiencies.

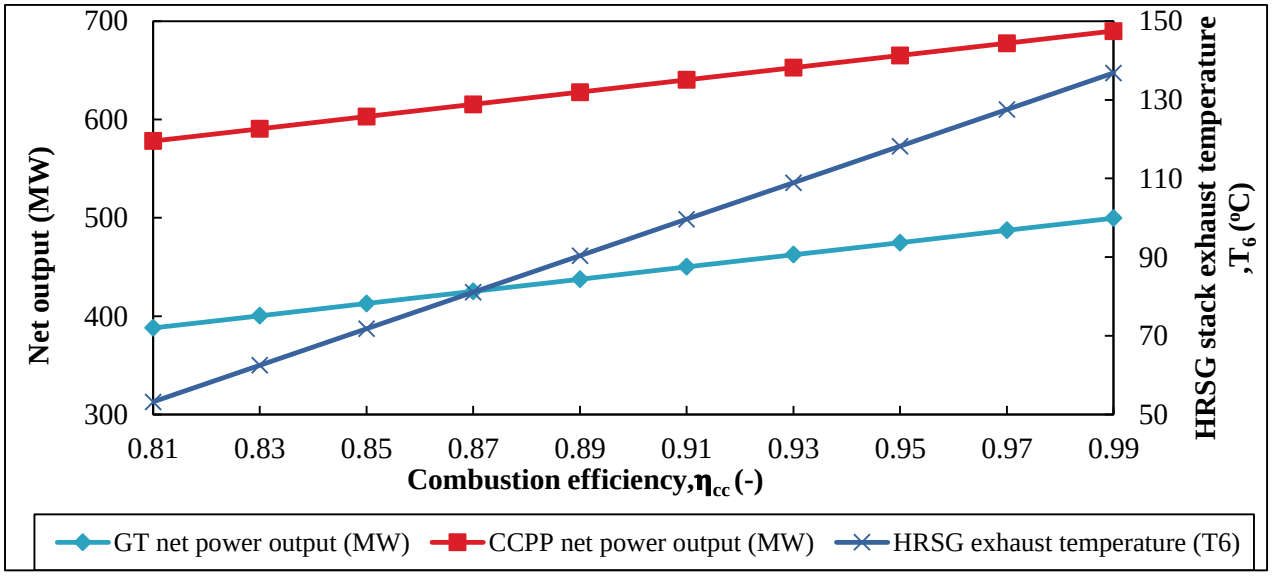

Figure 10. Effects of varying combustion efficiency on the net power outputs of the gas turbine and combined cycle power plants; and also on the HRSG stack exhaust temperature.

4. Conclusion

Ambient air conditions substantially affect the performance of combined gas- and steam-turbine power plants operating in hot and humid regions. A lot of previous works focused on improving the performance of combined gas- and steam- turbine power plant by inlet air cooling of the gas turbine cycle only. However, the performance of the steam turbine cycle fitted with air-cooled condensers are equally affected by the ambient conditions which

invariably impacts the overall performance of the combined cycle plant. In this study, the thermodynamic performance analysis of an existing combined cycle power plant retrofitted with a waste heat driven aqua lithium bromide absorption refrigerator for cooling the compressor and condenser inlet air streams has been conducted. This was achieved by performing the energy and exergy analysis of the integrated system and components. Using the operating data of an existing combined cycle power plant operating in the hot and humid tropical region of Nigeria, the results of the analysis show that by cooling the inlet air to the compressors to 15^{o}C, the net power output of the gas turbine cycle increases by 48.3MW, and by cooling the inlet air streams to the air-cooled steam condenser to 29^{o}C, the net power output of the steam turbine cycle increases by 1.4MW. The combined effect of compressor and condenser inlet air cooling is increase in the net power output, thermal and exergy efficiencies of the combined cycle plant by 7.7%, 8.1% and 7.5% respectively, and a drop in total exergy destruction rate and specific fuel consumption by 10.8% and 7.0% respectively. The stack flue gas exit temperature is reduced from 126^{o}C to 84^{o}C in the absorption refrigerator, thus reducing the exhaust heat discharge rate to the atmosphere. The COP and exergy efficiency of the refrigeration cycle are 0.60 and 27.0%, respectively. The relatively high exergy efficiency of the low grade waste heat operated LiBr-H_2O absorption refrigeration system is an indication of effective energy resource utilization. Results also show that the highest rate of exergy destruction in the CCPP occurs in the combustion chamber while the highest rate of exergy destruction in the absorption refrigeration cycle occurs in the evaporator followed by the absorber.

Parametric investigations reveal that the thermal and exergy efficiencies of the gas turbine, steam turbine and combined cycle power plants decrease with increase in ambient air temperature. The results for the special cases of the proposed plant studied agree very closely with those of previous works as well as with the measured data of the existing CCPP. It is shown that, as the combustion efficiency increases the net power outputs of the gas turbine and combined cycle power plants increase, and the temperature of the flue gases leaving the HRSG (and entering the ARC) increases, leading to increase in the grade of heat input to the adjoining absorption refrigeration unit. It is hoped that the results of this study will aid power plant operators in hot and humid regions seeking to make modifications for plant performance improvement.

References

Afam VI Combined Cycle Gas Turbine Plant (CCGT), 2015. *Plant operations report*, Afam, Nigeria.

Ahmadi, P., Dincer, I. & Rosen, M.A., 2012. Exergo-environmental analysis of an integrated organic Rankine cycle for trigeneration. *Energy Conversion and Management*, 64, pp.447–453.

Ahmadi, P., Dincer, I. & Rosen, M.A., 2013. Thermodynamic modeling and multi-objective evolutionary-based optimization of a new multigeneration energy system. *Energy Conversion and Management journal*, 76, pp.282–300.

Al-ibrahim, A.M. & Varnham, A., 2010. A review of inlet air-cooling technologies for

enhancing the performance of combustion turbines in Saudi Arabia. *Applied Thermal Engineering*, 30(14–15), pp.1879–1888.

Al-sulaiman, F.A., Dincer, I. & Hamdullahpur, F., 2012. Energy and exergy analyses of a biomass trigeneration system using an organic Rankine cycle. *Energy*, 45(1), pp.975–985.

Alhazmy, M.M. & Najjar, Y.S.H., 2004. Augmentation of gas turbine performance using air coolers. *Applied Thermal Engineering*, 24, pp.415–429.

Ameri, M. & Enadi, N., 2012. Thermodynamic modeling and second law based performance analysis of a gas turbine power plant (exergy and exergoeconomic analysis). *Journal of Power Technologies*, 92(3), pp.183–191.

Ameri, M. & Hejazi, S.. ., 2004. The study of capacity enhancement of the Chabahar gas turbine installation using an absorption chiller. *Applied Thermal Engineering*, 24, pp.59–68.

Ataei, A., Panjeshahi, M.H. & Gharaie, M., 2008. Performance evaluation of counter-flow wet cooling towers using exergetic analysis. *Transactions of the CSME/de la SCGM*, 32(3–4), pp.499–512.

Barigozzi, G. et al., 2015. Techno-economic analysis of gas turbine inlet air cooling for combined cycle power plant for different climatic conditions. *Applied Thermal Engineering*, 82, pp.57–67.

Bejan, A., Tsatsaronis, G., and Moran, M., 1996. *Thermal Design & Optimization*, New Jersey: John Wiley & Sons.

Boonnasa, S., Namprakai, P. & Muangnapoh, T., 2006. Performance improvement of the combined cycle power plant by intake air cooling using an absorption chiller. *Energy*, 31(12), pp.1700–1710.

Bustamante, J.G., Rattner, A.S. & Garimella, S., 2015. Achieving near-water-cooled power plant performance with air-cooled condensers. *Applied Thermal Engineering*, pp.1–10.

Cengel, Y.. & Boles, M.A., 2011. *Thermodynamics: An Engineering Approach* 7th ed., New York: McGraw-Hill Publishing Company.

Chuang, C. & Sue, D., 2005. Performance effects of combined cycle power plant with variable condenser pressure and loading. *Energy*, 30, pp.1793–1801.

Dawoud, B., Zurigat, Y.H. & Bortmany, J., 2005. Thermodynamic assessment of power requirements and impact of different gas- turbine inlet air cooling techniques at two different locations in Oman of different gas-turbine inlet air cooling techniques at two. *Applied Thermal Engineering*, 25, pp.1579–1598.

Dincer, I. & Ratlamwala, T., 2016. *Integrated Absorption Refrigeration Systems*, Switzerland: Springer.

Dinçer, I., Rosen, M. & Ahmadi, P., 2018. *Optimization of Energy Systems*, UK: Wiley.

Ehyaei, M.A. et al., 2015. Optimization of fog inlet air cooling system for combined cycle power plants using genetic algorithm. *Applied Thermal Engineering*, (76), pp.449–461.

Ersayin, E. & Ozgener, L., 2015. Performance analysis of combined cycle power plants: A case study. *Renewable and Sustainable Energy Reviews*, 43, pp.832–842.

Gadhamshetty, V. et al., 2006. Improving Air-Cooled Condenser Performance in Combined Cycle Power Plants. *Journal of Engineering Energy*, 132(2), pp.81–88.

Hosseini, R., Beshkani, A. & Soltani, M., 2007. Performance improvement of gas turbines of Fars (Iran) combined cycle power plant by intake air cooling using a media evaporative cooler. *Energy Conversion and Management*, 48, pp.1055–1064.

Jonsson, M. & Yan, J., 2005. Humidified gas turbines — a review of proposed and implemented cycles. *Energy*, 30, pp.1013–1078.

Kaushik, S.C. & Arora, A., 2009. Energy and exergy analysis of single effect and series flow double effect water – lithium bromide absorption refrigeration systems. *International Journal of Refrigeration*, 32(6), pp.1247–1258.

Khaliq, A., 2009. Exergy analysis of gas turbine trigeneration system for combined production of power heat and refrigeration. *International Journal of Refrigeration*, 32(3), pp.534–545.

Memon, A.G. et al., 2013. Thermo-environmental and economic analysis of simple and regenerative gas turbine cycles with regression modeling and optimization. *Energy Conversion and Management*, 76, pp.852–864.

Mohapatra, A.K., 2014. Thermodynamic assessment of impact of inlet air cooling techniques on gas turbine and combined cycle performance. *Energy*, (68), pp.191–203.

Muhsin, K. & Kaynakli, O., 2007. Second law-based thermodynamic analysis of water-lithium bromide absorption refrigeration system. *Energy*, 32, pp.1505–1512.

Nag, P.K., 2013. *Power Plant Engineering* 3rd ed., New Delhi: Tata McGraw Hill Education.

Najjar, Y.S.H. & Abubaker, A., 2015. Indirect Evaporative Combined Inlet Air Cooling With Gas Turbines as a Greening Technology. *International journal of refrigeration*, 59(2015), pp.235–250.

Nirmalakhandan, N., Gadhamshetty, V. & Mummaneni, A., 2008. Improving Combined Cycle Power Plant Performance. In *6th International Conference on Heat Transfer, Fluid Mechanics and Thermodynamics*. Pretoria, South Africa: HEFAT2008, pp. 1–6.

Oko, C.O.C. & Diemuodeke, E.O., 2010. Analysis of air-conditioning and drying processes using spreadsheet add-in for psychrometric data. *Journal of Engineering Science and Technology Review*, 3(1), pp.7–13.

Oko, C.O.C. & Njoku, I.H., 2017. Performance analysis of an integrated gas- , steam- and organic fluid-cycle thermal power plant. *Energy*, 122, pp.431–443.

Oko, C.O.C. & Ogoloma, O.B., 2011. Generation of a typical meteorological year. *Journal of Engineering Science and Technology*, 6(2), pp.204–214.

Popli, S., Rodgers, P. & Eveloy, V., 2013. Gas turbine efficiency enhancement using waste heat powered absorption chillers in the oil and gas industry. *Applied Thermal Engineering*, 50(1), pp.918–931.

Ramani, A.R. V, Paul, B.A. & Saparia, D.A.D., 2011. Performance Characteristics of an Air-Cooled Condenser Under Ambient Conditions. In *International Conference on Current Trends in Technology 'NUiCONE – 2011*. Ahmedabad: Institute of technology, Nirma university, pp. 382–481.

Saravanamuttoo, H.I.., Cohen, H. & Rogers, G.F.., 1996. *Gas Turbine Theory* 4th ed., London: Longman.

Singh, O.K., 2016. Performance enhancement of combined cycle power plant using inlet air cooling by exhaust heat operated ammonia-water absorption refrigeration system. *Applied Energy*, 180, pp.867–879.

Talbi, M.M. & Agnew, B., 2000. Exergy analysis : an absorption refrigerator using lithium bromide and water as the working fluids. *Applied Thermal Engineering*, 20, pp.619–630.

Tiwari, A.K., Hasan, M.M. & Islam, M., 2013. Exergy Analysis of Combined Cycle Power Plant : NTPC Dadri , India. *International Journal of Thermodynamics*, 16(1), pp.36–42.

Touaibi, R. et al., 2013. Parametric study and exergy analysis of solar water- lithium bromide absorption cooling system. *International Journal of Exergy*, x(x), pp.1–16.

Yang, L. et al., 2012. Thermal- flow characteristics of the new wave- finned flat tube bundles in air-cooled condensers. *International Journal of Thermal Sciences*, 53, pp.166–174.

Zaki, G.M., Jassim, R.K. & Alhazmy, M.M., 2011. Energy , Exergy and Thermoeconomics Analysis of Water Chiller Cooler for Gas Turbines Intake Air Cooling. *Smart Grid and Renewable Energy*, 2, pp.190–205.